Characterization of river delta shorelines

N. Geleynse,[1] V. R. Voller,[1,2] C. Paola,[1,3] and V. Ganti[1,2]

Received 21 June 2012; revised 27 July 2012; accepted 30 July 2012; published 7 September 2012.

[1] Coastline shape is among the basic geometric properties of the Earth's surface, yet defining and quantifying coastline shape precisely remains challenging. Here we propose new methods, based on the dilation and erosion operators of mathematical morphology (MM), for the characterization of delta shorelines, a class of open coasts. We demonstrate the suitability of MM-based methods for noise removal and shoreline identification from digital images of river deltas of varying geometric complexity. We also show that a global, a regional and a local shoreline parameter provide a first step in distinguishing among river, wave, and tidal dominated delta shapes. **Citation:** Geleynse, N., V. R. Voller, C. Paola, and V. Ganti (2012), Characterization of river delta shorelines, *Geophys. Res. Lett.*, *39*, L17402, doi:10.1029/2012GL052845.

1. Introduction

[2] Fundamentally, a shoreline is a geometric entity that carries the signature of the processes that create it. The interplay of terrestrial and basinal processes that sculpt shorelines is especially prominent in river deltas, of which hundreds of striking examples are now accessible through the global database of satellite images. Delta planform information, although conditioned by the imaging process itself [*Burrough and McDonnell*, 1998], is more than adequate to allow initial analysis of quantitative shoreline geometry. Moreover, altimetric data of deltas, hence their shorelines, is yet limited, underlining the need for methods to extract information from gridded planform imagery [e.g., *Geleynse et al.*, 2011]. In addition, comparison between geometric digital data and digital data on the spectral response of geometric surfaces of, for example, different lithology, stratigraphy and vegetation, will provide insights into the functioning of landscapes, hence rendering development of techniques for object detection highly relevant.

[3] In view of the dynamic nature of the land-water interface, and its subtlety on low-gradient depositional coasts, the definition of a shoreline remains challenging [*Shaw et al.*, 2008], even for a seemingly simple "closed" shoreline [*Aarninkhof et al.*, 2003], despite the common use of shoreline as a marker for environmental change in engineering, geological and climatic studies as well as its importance to society. This becomes even more evident for river delta shorelines which, due to the presence of channels, are discontinuous, thus requiring objective criteria for their delineation. This study proposes such criteria, providing an alternative to the opening angle method (OAM) developed in *Shaw et al.* [2008].

2. Mathematical Morphology

[4] Our main idea is to use the morphological closing operator from mathematical morphology theory [*Serra*, 1982] to define the wetted or open part of shorelines of river deltas by effectively "closing" distributary channels that protrude the otherwise continuous land-water interface. Moreover, the proposed method allows for quantification of the range of potential delta shoreline position, thereby characterizing the shoreline roughness. This in turn leads to quantitative measures to differentiate among river deltas based on their exterior, thereby enabling quantification of the classical wave-tide-river classification system for river deltas [*Galloway*, 1975].

[5] Next, we briefly present the principles of mathematical morphological operators relevant to the present study. Mathematical morphology is established to the point where appropriate code for the elementary operations is available in software packages; in the current work MATLAB was used in this role. Previous application of MM include shoreline tracking along the continuous Normandy coast based on multispectral imagery [*Puissant et al.*, 2008], water depth determination for synthetic data sets of a wave crest field [*Martín et al.*, 1999] and grain size characterization of river bed samples [*Graham et al.*, 2005]. To our knowledge, this is the first study employing MM for shoreline identification for river deltas.

[6] MM theory has different definitions [*Serra and Vincent*, 1992, and references therein]. For our purposes, it is a set of filters based on set theory. In contrast to linear filters such as convolution, morphological operations are nonlinear, and are directly related to object shape. In MM, sets represent the objects or shapes that are manifested on an image of any dimension, e.g., the set of all white (foreground) pixels in a black and white image. Though applicable to sets of any dimension, MM transformations are most easily understood for the two-dimensional binary case. Therefore, we first consider their application to plan view binary images of deltas.

3. Delta Shorelines

3.1. Application of MM to a Schematized Delta

[7] The elementary operations in MM are dilation and erosion [*Serra*, 1982] (Figures 1a–1d). In combination with another operation, known as reconstruction [*Vincent*, 1993], shorelines can be obtained. Here, we explain and illustrate these three operations.

[1]National Center for Earth-Surface Dynamics, St. Anthony Falls Laboratory, University of Minnesota, Twin Cities, Minneapolis, Minnesota, USA.
[2]Department of Civil Engineering, University of Minnesota, Twin Cities, Minneapolis, Minnesota, USA.
[3]Department of Earth Sciences, University of Minnesota, Twin Cities, Minneapolis, Minnesota, USA.

Corresponding author: N. Geleynse, National Center for Earth-Surface Dynamics, St. Anthony Falls Laboratory, University of Minnesota, Twin Cities, 2 Third Ave., SE, Minneapolis, MN 55414, USA. (ngeleyns@umn.edu)

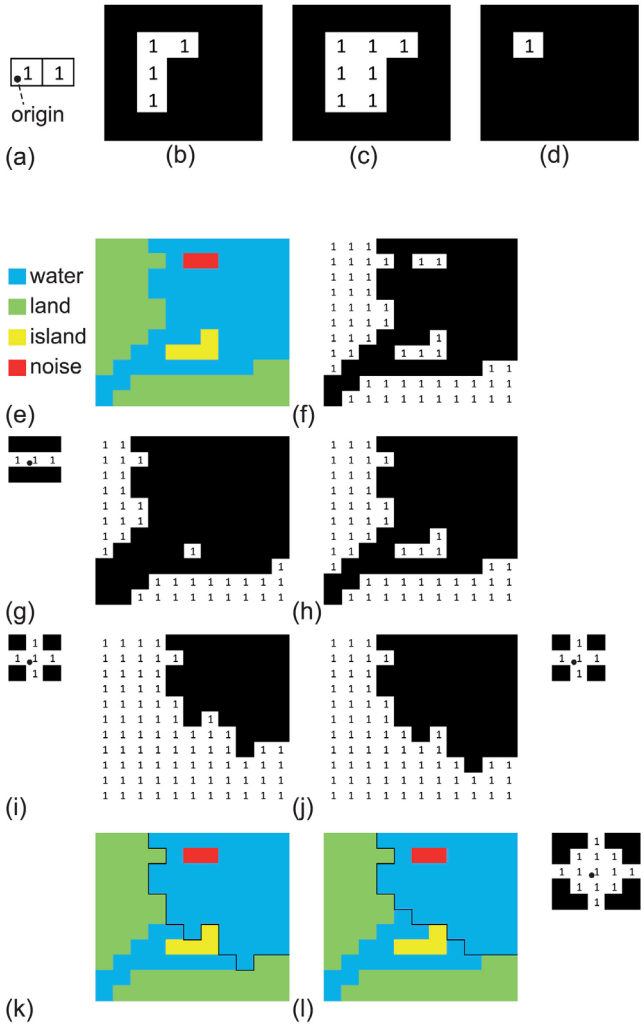

Figure 1. Example of the basic operations of MM: (a) Structure element (S), (b) input image (I), (c) dilation of I by S, and (d) erosion of I by S, and their use for shoreline extraction of a binary image. (e) A hypothetical river delta, where colors would correspond to colors or gray levels. (f) A binarized version of Figure 1e. (g) Erosion of Figure 1f by shown S. (h) Reconstruction of Figure 1g. (i) Dilation of Figure 1h by shown S. (j) Erosion of Figure 1i by shown S. (k) Example shoreline (black). (l) Example shoreline for a larger S in Figures 1i and 1j. The larger S, the smoother the resulting shoreline.

[8] First, a shape S is defined as a set of contiguous pixels with one pixel identified as the origin (Figure 1a). This shape, also known as a structure element [*Haralick et al.*, 1987], is moved over a discrete two-dimensional space, $\mathbb{Z}^2$. In each case that the origin coincides with a pixel $i \in I$, where I is the image (Figure 1b), we record the shape S_i. The dilation of I is then the union of all these shapes (Figure 1c);

$$I \oplus S = \bigcup_{i \in I} S_i \tag{1}$$

[9] Erosion is the morphological dual (counterpart) to dilation [*Haralick et al.*, 1987]. In contrast to dilation, this operation, not to be confused with its geomorphological meaning, essentially shrinks the objects in the image. Analogous to dilation, a shape S is defined and then moved over $\mathbb{Z}^2$. In each case that the origin coincides with a pixel $i \in I$, it is assessed whether the shape S matches the shape present in I at that pixel. If not, the pixel is excluded from the set. Accordingly, the erosion of I is the intersection of all translations of I by the pixels $-s$, where $s \in S$ (Figure 1d) and where the minus sign corresponds to reflecting all pixels of S about its origin;

$$I \ominus S = \bigcap_{s \in S} I_{-s} \tag{2}$$

[10] Reconstruction refers to the operation of noise removal such that natural large-scale objects can be segmented, here deep water and the river delta. First, a shape S is defined based on analyzing the shape and size of the noise in I (Figures 1e–1f). I is then eroded by S (Figure 1g). The shapes in this eroded image J are then restored to their original shape in I by collecting all the neighboring pixels and those that can be connected unobstructedly to them, for which $i \in I$, for each $j \in J$ (Figure 1h).

[11] To obtain a shoreline, it is not sufficient to merely dilate the reconstructed image (Figure 1h), because of the extensivity property of dilation [*Haralick et al.*, 1987]. However, the sequential application of dilation and erosion overcomes such arbitrary expansion of the land-water interface. In fact, the dilation of an image I by S followed by erosion of the resulting image is an operation referred to as morphological closing;

$$I \bullet S = (I \oplus S) \ominus S \tag{3}$$

with its dual (counterpart) being known as opening [*Haralick et al.*, 1987].

[12] Application of the closing operator to our synthetic river delta (Figure 1h), i.e., eroding the dilated image (Figures 1i–1j) results in a continuous shoreline (Figure 1k). Using a larger S yields a smoother shoreline (Figure 1l). Generally, we suggest scaling S with channel size (and obviously with image resolution), pointing at the key physical assumption of the method, namely that shoreline roughness is slaved to the roughness of the channel network, a condition that we expect is met for many natural cases. Further, we propose a disk-shaped S to be most appropriate for deltas, because of the typical curvilinear nature of their component objects: channels, bars and islands.

[13] Finally, we note an important property of the closing and opening transformations, namely its so-called idempotency [*Haralick et al.*, 1987], meaning that reapplication of the transformation does not alter the previously obtained (closed) image. Accordingly, an otherwise arbitrary choice for the number of iterations vanishes.

3.2. Application of MM to Real-World Deltas

[14] While application of morphological operators to binary imagery can be very effective, direct binarization of grayscale or multispectral imagery is not always straightforward. The problem becomes readily apparent for a radar image of the modern tide-influenced Mahakam River Delta (Figure 2b) where image corruption by noise complicates binarization. However, binarization is not necessary *per se*, since the binary

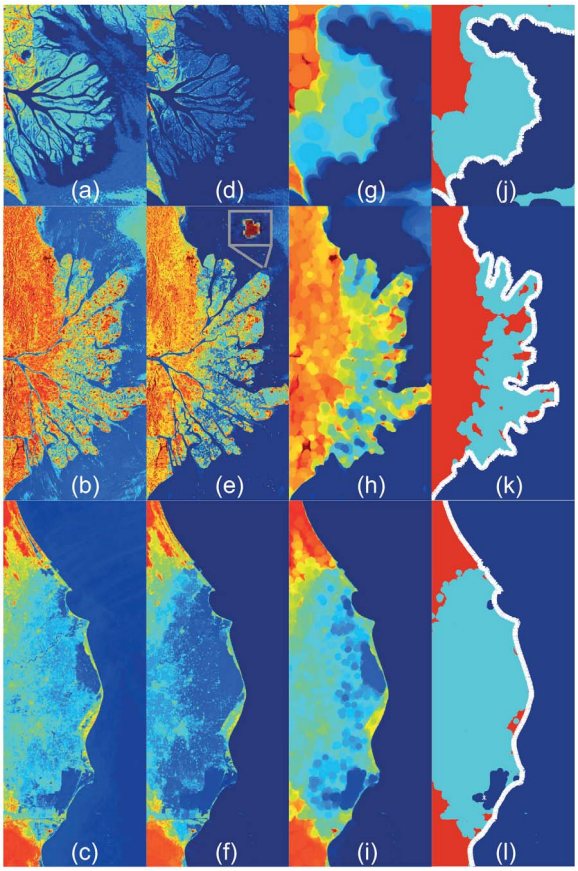

Figure 2. Shoreline extraction from grayscale images. (a) A grayscale image (NIR band) of a satellite image of the Wax Delta, 11/17/2005 (Credit: NASA/Landsat) (resolution ≈ 50 m); (b) radar image (C-band) of the Mahakam delta, 11/12/2009 (Credit: ESA/Chelys) (resolution ≈ 60 m); and (c) satellite image (blue band) of the Nile delta, 10/13/2010 (Credit: NASA/Chelys) (resolution ≈ 200 m). All grayscale images are mapped to the "jet"-colorspace for visualization. (d–f) Reconstructed images from marker images that are obtained by subtraction of a constant (50, 100 and 30 respectively) from Figures 2a–2c, respectively. The inset in Figure 2e highlights noise that is removed by reconstruction of the above-reconstructed image from its eroded image (here with a flat disk-shaped structure element of R = 5 pixels). (g–i) Closing of Figures 2d–2f by flat disk-shaped structure elements (radii of 15 pixels). (j–l) Clustering of Figures 2g–2i into "water", "land-water" and "land" classes by *Otsu* [1979]'s method. The extracted shorelines are indicated by white lines.

morphological operators have their grayscale counterparts [*Haralick et al.*, 1987].

[15] In grayscale morphology, the elementary dilation and erosion operations are extended to comprise a maximum and minimum operation, respectively. Let F and H be the domains of the grayscale image, $f(x, y)$, and the grayscale structure element, $h(m, n)$, respectively, the grayscale dilation of f by h is defined according to [*Haralick et al.*, 1987]

$$(f \oplus_g h)(x,y) = \max\{f(x-m, y-n) + h(m,n)\} \quad (4)$$

for all $(m, n) \in H$ and $(x - m, y - n) \in F$ with the grayscale erosion being defined similarly;

$$(f \ominus_g h)(x,y) = \min\{f(x+m, y+n) - h(m,n)\} \quad (5)$$

for all $(m, n) \in H$ and $(x + m, y + n) \in F$. For the present study, we take a flat disk-shaped, $h(m, n) = 0$, accordingly, equations (4) and (5) reduce to a maximum and minimum operator, respectively. Informally, grayscale dilation of an image with a flat disk-shaped structure element generally results in the growth of bright regions which are surrounded by dark regions, whereas darker regions will shrink, and vice versa for grayscale erosion, depending on how the shapes and sizes of geometric components relate to the structure element.

[16] Having expressions for grayscale dilation and erosion, grayscale closing is defined analogously to the binary case [*Haralick et al.*, 1987]:

$$f \bullet_g h = (f \oplus_g h) \ominus_g h \quad (6)$$

[17] Figures 2a, 2b and 2c show a satellite image of the river-dominated Wax Lake Delta, a radar image of the tide-influenced Mahakam River Delta and a satellite image of the modern wave-dominated Nile River Delta, respectively. For

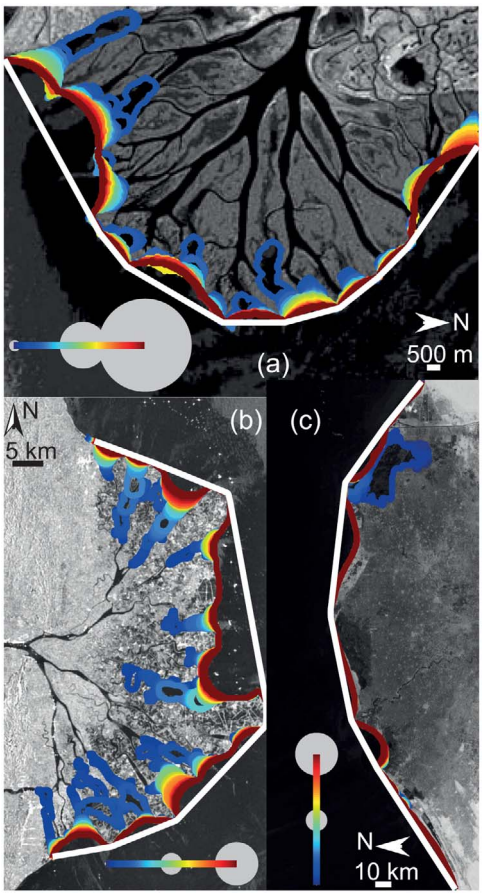

Figure 3. (a) Wax, (b) Mahakam and (c) Nile shorelines (colors) for different R (e.g., gray disks), and obtained as outlined in Figure 2. Note that R can be even larger, however requiring image resizing. Convex hulls (excluding segments connecting delta shoreline ends) are indicated.

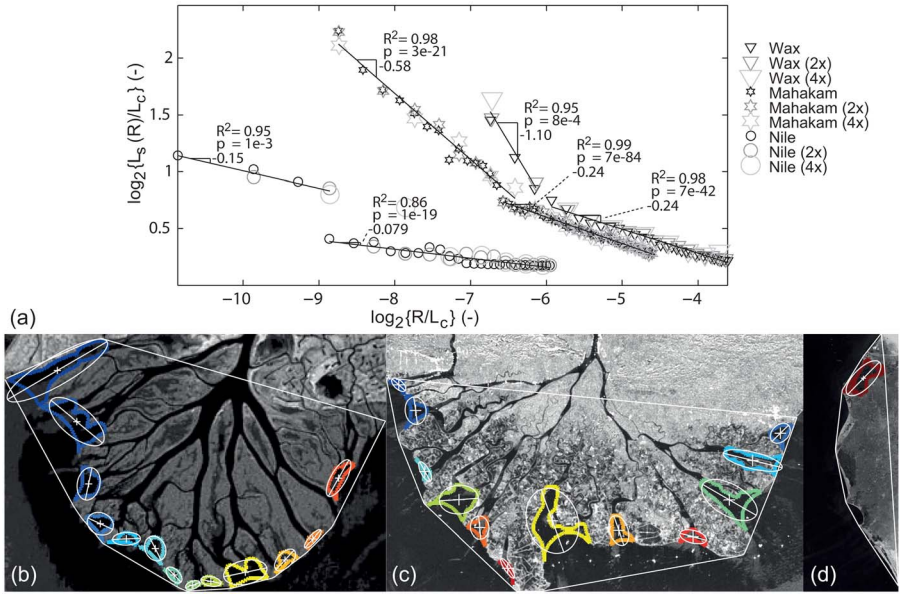

Figure 4. (a) Plot of normalized delta shoreline length $L_s(R)/L_c$ against R/L_c (and regression lines with slopes, R^2 and corresponding p-values) for three cases and for three image resolutions (legend), obtained by bicubic interpolation, demonstrating the consistency of our method. (b–d) Roughness objects for the Wax, Mahakam and Nile cases, defined by a shoreline obtained for a mean R of all R before the scaling break in Figure 4a and a shoreline obtained for R just before the scaling break. These objects, after filtering those smaller than 25% of their mean size, are approximated by ellipses (white lines) which have the same second moment. Their centroids and longest principal axii are indicated. Shorelines' convex hulls are also shown.

all cases, it can be seen that deep water is not represented by a uniform gray-level (Figures 2a–2c). Generally, ignorance of these local intensity fluctuations would lead to inclusion of false shoreline paths. Accordingly, akin to the binary case (Figure 1), application of a reconstruction operator is necessary. First, the complement of the original grayscale image f (Figures 2a–2c) is taken such that the intensity fluctuations in deep water correspond to local maxima (with respect to the entire image), where the background is a regional maximum. The resulting image is denoted by k. Next, we subtract a constant, based on the intensity fluctuations from k to result in an image p, the "marker" image [*Vincent*, 1993]. The reconstruction of k from p, denoted by q, is a dilation of p, conditioned by k. For the mathematics involved, refer to *Vincent* [1993, Figures 8 and 12]. Then, we take the complement of q, denoted by r (Figures 2d–2f). The suitability of the use of the reconstruction operator can be observed (Figures 2d–2f) in that it suppresses or completely removes (shore-detached) sediment plumes that are obviously not part of the shoreline, however typically having a spectral signature that is not easily distinguishable from that of (wetted parts of) islands and bars.

[18] Subsequently, for the Mahakam case, clouds entail noise which is manifested by local maxima in r (Figure 2e, inset). Accordingly, we erode r with a flat h of which size and shape matches the characteristic size and shape of these noisy pixels, followed by a reconstruction of r from this eroded image.

[19] For all three cases, the reconstructed image is closed by a flat disk-shaped structure element of a given radius (Figures 2g–2i). Subsequently, we use a well-known histogram-based cluster method [*Otsu*, 1979], followed by a merging of the resulting "land" and "land-water interface" (delta) classes (Figures 2j–2l). The shoreline is then obtained by subtraction of the eroded clustered binary image (with S of radius = 1 pixel) from the clustered binary image itself (white lines in Figures 2j–2l). The delta shoreline pixels are listed based on the Moore-Neighbor algorithm [*Gonzalez et al.*, 2004] and with manual selection of their ends.

[20] Finally, we note that available images are usually not monochromatic, but contain more information, though the contrast between land and water is often most pronounced

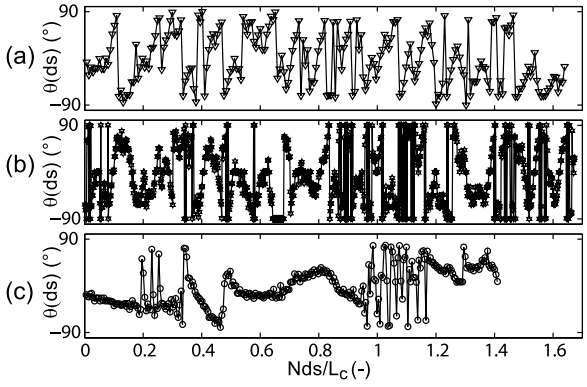

Figure 5. Plots of local change of tangent vector $d\theta$ against normalized arc length Nds/L_c, where N denotes the number of arc lengths, for the (a) Wax, (b) Mahakam and (c) Nile river delta shorelines based on fitted cubic splines. These shorelines are obtained for the R-value next to the scaling breaks in Figure 4a. For the Wax and Mahakam cases, ds = 200 m, for the Nile delta, ds = 2000 m. Taking identical ds for all cases does not alter the conclusions, but the Nile shoreline likely contains low-amplitude (≈25°) noise at small scales as can be inferred from its planform step-wise structure (here not shown).

for one of the spectral bands, such as NIR. Other approaches employ arithmetic operations like division and subtraction of spectral bands, yielding a "grayscale image", e.g., the Normalized Difference Vegetation Index for mapping desertification. Alternatively, a grayscale image can be selected based on the Hotelling Transform [*Gonzalez et al.*, 2004], then applying the closing operator to the component which contains most of the energy.

4. Shoreline Characterization

[21] An important characteristic of delta shorelines is discontinuity associated with the presence of channels. Closing images of deltas by structure elements of different radii (R) provides a means to quantify geometric statistics of these openings; distributary channel mouths, tidal channels, backbarrier lagoons and embayments (Figure 3). As a first global measure, we propose a delta shoreline sinuosity, defined as a normalized shoreline length; $L_s(R)/L_c$, where $L_s(R)$ is the length of the delta shoreline (summed distances between neighboring pixels) corresponding to R. We suggest taking the length of the shoreline's convex hull for L_c, i.e. using the convex hull as a reference shoreline (Figure 3). The convex hull is defined by the extreme shoreline points that are potentially most exposed to basinal forcings, and it effectively sets the maximum roughness of the delta shoreline. Moreover, as can be readily deduced from Figure 3, the convex hull is virtually invariant to R.

[22] The resulting plot of $L_s(R)/L_c$ against R/L_c reveals interesting scaling behaviour (Figure 4a). First, the windwave-dominated shoreline of the Nile delta is most smooth at all examined ranges of R, compared to the river and tide-influenced river delta shorelines (cf. slopes in Figure 4a). Further, it depicts a discontinuity which is directly related to the existence of a backbarrier lagoon which is not entirely disconnected from deeper water (Figures 3c and 4d). Accordingly, we find a measure to formally define a transition from a river-dominated to a wave-dominated delta shoreline or vice versa. In the limit, a wave-dominated river delta would feature a continuous barrier shoreline that fully encloses water bodies (lagoons). In that case, the roughness of the shoreline is set by cuspate-shaped river mouths, here the Rosetta and Damietta promontories. In contrast, the river and tide-influenced delta shorelines are rougher and also feature scaling breaks (Figure 4a). These scaling breaks are related to characteristics of the channel network, where meandering (Figure 3b) provides excess length as well as to topographic lows such as patches of easily-flooded deltaplain (Figures 3a and 3b). Since lengths of naturally-closed objects such as bar faces as well as L_c do not significantly differ for R (Figure 3), the slope beyond the scaling break in Figure 4a (Mahakam delta) directly provides a measure for the degree of funnelling (planform divergence) of tide-influenced distributary and tidal channels.

[23] The scaling breaks allow for the definition and quantification of roughness objects on a delta shoreline. Here, we define objects by the space enclosed by a low-R shoreline and a maximum-R shoreline (Figures 4b–4d), while inherent uncertainty is incorporated in our shape descriptors by taking different low-R. Having identified these regional objects, we represent them by ellipses that have identical second moments (Figures 4b–4d). The distributions of their eccentricity, α, combined with the orientation of the longest principal axis of these ellipses with respect to the nearest convex hull segment, β, enable classification of river delta shorelines. For the Nile delta, only one object can be defined, pointing at the fact that its shoreline is almost entirely continuous. The Wax and Mahakam delta shorelines can be differentiated; the mean eccentricity of all ellipses corresponding to all R before the scaling break (Figure 4a) is about equal for both cases; $\bar{\alpha} = 0.81 \pm 0.015$ and 0.81 ± 0.026, respectively, however, $\bar{\beta} = 23.5 \pm 7.3°$ and $49.8 \pm 10.4°$, respectively, meaning that objects on the tidally-influenced delta shoreline are relatively more oriented perpendicular to the shoreline.

[24] Finally, we fit splines to the raster Wax, Mahakam and Nile delta shorelines (Figure 5), which allows for their differentiation based on a local measure. Analyzing the local change of the tangent vector ($d\theta$) as a function of normalized arc length (Nds/L_c), we refine our conclusions based on the shoreline's sinuosity (Figure 4a); the Wax shoreline depicts the highest directional variability at relatively small scales, while the Mahakam shoreline depicts significant directionality at larger scales. The Nile shoreline is smooth at small scales, however, it has large-scale directional variability associated with the presence of abandoned delta lobes.

[25] Future work should focus on further testing and expanding of these measures as well as including a detailed comparison with the OAM [*Shaw et al.*, 2008]. We do note, however, that immediate advantages in the MM approach is its efficient computation and the introduction of an explicit length scale, S, allowing for a coupling between a delta's exterior and its interior geometry, e.g., the channel network.

[26] **Acknowledgments.** This contribution was supported by NCED, NSF (EAR-0120914) and by Deltares, Netherlands. We thank D. Edmonds and an anonymous reviewer.

[27] The Editor thanks Douglas Edmonds and an anonymous reviewer for their assistance evaluating this paper.

References

Aarninkhof, S. G. J., I. L. Turner, T. D. T. Dronkers, M. Caljouw, and L. Nipius (2003), A video-based technique for mapping intertidal beach bathymetry, *Coastal Eng.*, *49*(4), 275–289.

Burrough, P. A., and R. A. McDonnell (1998), *Principles of GIS*, 333 pp., Oxford Univ. Press, Oxford, U. K.

Galloway, W. E. (1975), Process framework for describing the morphologic and stratigraphic evolution of deltaic depositional systems, in *Deltas: Models for Exploration*, vol. 2, pp. 87–98, Houston Geol. Soc., Houston, Tex.

Geleynse, N., J. E. A. Storms, D. J. R. Walstra, H. R. A. Jagers, Z. B. Wang, and M. J. F. Stive (2011), Controls on river delta formation; insights from numerical modelling, *Earth Planet. Sci. Lett.*, *302*(1), 217–226.

Gonzalez, R. C., R. E. Woods, and S. L. Eddins (2004), *Digital Image Processing Using MATLAB*, Pearson Prentice Hall, Upper Saddle River, N. J.

Graham, D. J., S. P. Rice, and I. Reid (2005), A transferable method for the automated grain sizing of river gravels, *Water Resour. Res.*, *41*, W07020, doi:10.1029/2004WR003868.

Haralick, R. M., S. R. Sternberg, and X. Zhuang (1987), Image analysis using mathematical morphology, *IEEE Trans. Pattern Anal. Machine Intell.*, *9*(4), 532–550.

Martín, M. L., M. Y. Luna, F. Valero, S. M. Lea, and M. Lybanon (1999), Finding water depths from synthetic remotely sensed images, in *International Conference on Image Analyis and Processing: Proceedings of the 10th International Conference*, pp. 862–867, Inst. of Electr. and Electron. Eng., Los Alamitos, Calif.

Otsu, N. (1979), A threshold selection method from gray-level histograms, in *IEEE Trans. Syst. Man Cybern.*, *9*, 62–66.

Puissant, A., S. Lefèvre, and J. Weber (2008), Coastline extraction in VHR imagery using mathematical morphology with spatial and spectral knowledge, in *Int. Arch. Photogramm. Remote Sens. Spatial Inf. Sci.*, *37*, 1305–1310.

Serra, J. (1982), *Image Analysis and Mathematical Morphology*, Academic, London.

Serra, J., and L. Vincent (1992), An overview of morphological filtering, *Circuits Syst. Signal Process.*, *11*(1), 47–108.

Shaw, J. B., M. A. Wolinsky, C. Paola, and V. R. Voller (2008), An image-based method for shoreline mapping on complex coasts, *Geophys. Res. Lett.*, *35*, L12405, doi:10.1029/2008GL033963.

Vincent, L. (1993), Morphological grayscale reconstruction in image analysis: Applications and efficient algorithms, *IEEE Trans. Image Process.*, *2*, 176–201.